

---

# THE INITIAL CHARGE SEPARATION STEP IN OXYGENIC PHOTOSYNTHESIS

---

Yusuke Yoneda,<sup>1,2,5</sup> Eric A. Arsenault,<sup>1,2,3</sup> Kaydren Orcutt,<sup>1,2</sup> Masakazu Iwai,<sup>2,4</sup> Graham R. Fleming,<sup>1,2,3,\*</sup>

<sup>1</sup>Department of Chemistry, University of California, Berkeley, CA 94720, USA

<sup>2</sup>Molecular Biophysics and Integrated Bioimaging Division,

Lawrence Berkeley National Laboratory, Berkeley, CA 94720, USA

<sup>3</sup>Kavli Energy Nanoscience Institute at Berkeley, Berkeley, CA 94720, USA

<sup>4</sup>Department of Plant and Microbial Biology, University of California, Berkeley, CA 94720, USA

<sup>5</sup>Present Address: Research Center of Integrative Molecular Systems,  
Institute for Molecular Science, National Institute of Natural Sciences, Okazaki, Aichi, 444-8585, Japan

\*grfleming@lbl.gov

September 24, 2021

## ABSTRACT

Photosystem II is crucial for life on Earth as it provides oxygen as a result of photoinduced electron transfer and water splitting reactions. The excited state dynamics of the photosystem II-reaction center (PSII-RC) has been a matter of vivid debate because the absorption spectra of the embedded chromophores significantly overlap and hence it is extremely difficult to distinguish transients. Here, we report the two-dimensional electronic-vibrational spectroscopic study of the PSII-RC. The simultaneous resolution along both the visible excitation and infrared detection axis is crucial in allowing for the character of the excitonic states and interplay between them to be clearly distinguished. In particular, this work demonstrates that the mixed exciton-charge transfer state, previously proposed to be responsible for the far-red light operation of photosynthesis, is characterized by the  $\text{Chl}_{\text{D1}}^+\text{Phe}^-$  radical pair and can be directly prepared upon photoexcitation. Further, we find that the initial electron acceptor in the PSII-RC is Phe, rather than  $\text{P}_{\text{D1}}$ , regardless of excitation wavelength.

## 1 Introduction

Photosynthesis, the green engine of life on Earth, produces molecular oxygen by using the light-driven water-plastoquinone oxidoreductase enzyme known as photosystem II.<sup>1-3</sup> The photosystem II-reaction center (PSII-RC) is one of the smallest photosynthetic components which can undergo charge separation (CS) and thus is an ideal model system to investigate the underlying mechanism of the initial light-energy conversion process of photosynthesis.<sup>4-6</sup> The PSII-RC consists of six pigments as central cofactors—two special pair chlorophylls ( $\text{P}_{\text{D1}}$  and  $\text{P}_{\text{D2}}$ ), two accessory chlorophylls ( $\text{Chl}_{\text{D1}}$  and  $\text{Chl}_{\text{D2}}$ ), and two pheophytins ( $\text{Phe}_{\text{D1}}$  and  $\text{Phe}_{\text{D2}}$ )—arranged in a quasi-symmetric geometry (Figure 1a).<sup>7,8</sup> These six molecules are generally referred to as RC pigments. In addition, there are two peripheral antenna Chls which are denoted as  $\text{Chlz}_{\text{D1}}$  and  $\text{Chlz}_{\text{D2}}$ . Despite the similarity of the pigment arrangement in the D1 and D2 branches, electron transfer only proceeds along the D1 pigments. The specifics of how CS proceeds in the PSII-RC is, however, a matter of vivid debate. In particular, there remains a long-standing discussion concerned with whether the initial electron acceptor is  $\text{P}_{\text{D1}}$ <sup>9,10</sup> or  $\text{Phe}_{\text{D1}}$ ,<sup>11-13</sup> i.e. whether the initial radical pair is ( $\text{P}_{\text{D2}}^+\text{P}_{\text{D1}}^-$ ) or ( $\text{Chl}_{\text{D1}}^+\text{Phe}_{\text{D1}}^-$ ). The uncertainty here is a consequence of the many closely spaced excitonic states arising from pigment-pigment interactions in the PSII-RC such that no observable structure is present even in the electronic linear absorption spectrum at cryogenic temperatures.<sup>14-16</sup>

To this end, the excited state dynamics of the PSII-RC has been the focus of extensive spectroscopic interest spanning over three decades. These works have included time-resolved fluorescence,<sup>17,18</sup> transient absorption,<sup>9,10,13,19-21</sup> optical

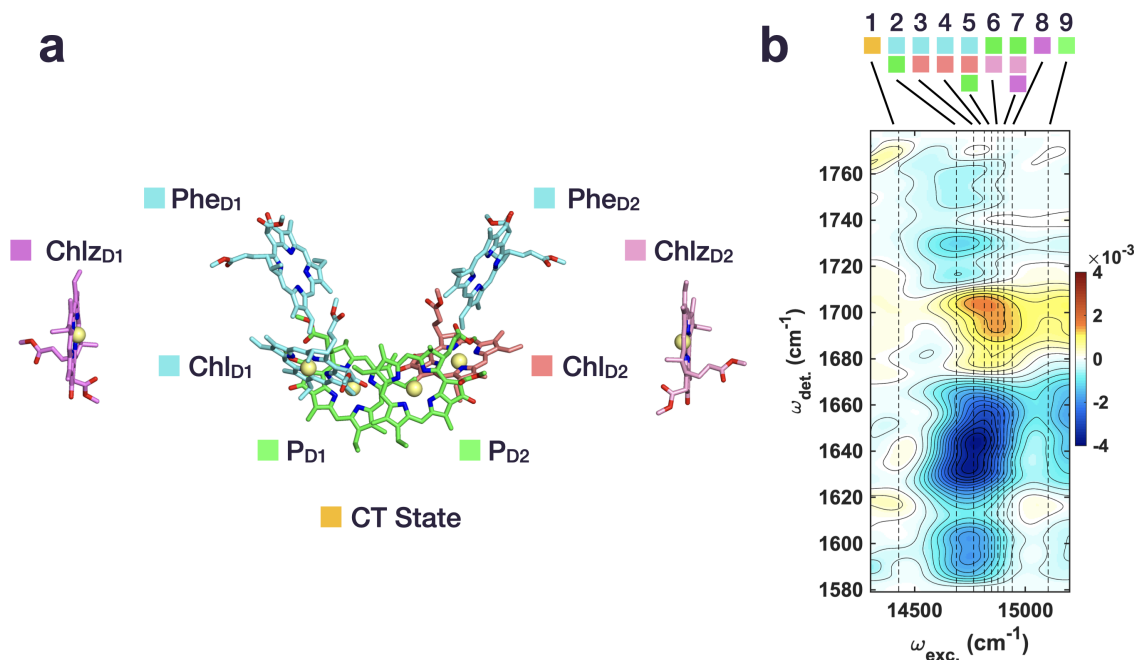


Figure 1: Structure and 2DEV spectrum of the PSII-RC. (a) Pigment arrangement of the PSII-RC depicted based on the crystal structure (3WU2) reported by Umena et al.<sup>8</sup> (b) 2DEV spectrum of the PSII-RC at 170 fs. Positive contours (red/yellow) indicate ground state bleach (GSB) features and negative contours (blue) indicate photoinduced absorption (PIA) features. The vertical dotted lines show the zero phonon exciton transition energies based on the model by Novoderezhkin et al.<sup>35</sup> Contour levels are drawn in 5% intervals. Colored squares on the top indicate the dominant pigments participating in each excitonic state as labeled in (a).

photon-echo,<sup>12</sup> visible pump-mid infrared (IR) probe,<sup>11</sup> and two-dimensional electronic spectroscopy (2DES)<sup>14,22–24</sup> studies. While electronic spectroscopies acutely suffer from a lack of spectral resolution in regards to the PSII-RC, the implementation of mid-IR spectroscopy has proven to be highly advantageous in addressing issues related to spectral congestion.<sup>25–28</sup> In particular, the keto and ester CO stretching modes of Chl and Phe show unique signatures in the mid-IR region depending on the local protein environment, electronic structure, and ionic states.<sup>11,29–33</sup> Additionally, the amide I modes of the backbone protein can be used as sensitive reporters for the electron transfer.<sup>11,31</sup> These were notably demonstrated by Groot et al. in a visible pump-mid IR probe study of the PSII-RC where it was suggested that the initial electron acceptor was Phe based on its distinguishing vibrational structure.<sup>11</sup> However, the spectral resolution along the detection axis alone was not enough to disentangle the distinct excitonic contributions and dynamics or definitively assign the initial electron acceptor.

Many theoretical models have been developed in order to aid in experimental interpretation and to elucidate the nature the electronic states at difference absorption wavelengths. Particularly, Stark spectroscopy suggests that the absorption spectrum of PSII is not characterized by purely excitonic states, rather it is composed of mixed exciton-charge transfer (CT) states possibly including contributions from  $(\text{Chl}_{\text{D1}}^{\delta+}\text{Phe}_{\text{D1}}^{\delta-})^*$  and  $(\text{P}_{\text{D2}}^{\delta+}\text{P}_{\text{D1}}^{\delta-})^*$ .<sup>34</sup> In an attempt to model this, one of the most sophisticated exciton models of the PSII-RC takes into account eight pigments—the six RC and two peripheral pigments—and one CS state.<sup>35</sup> Even in this model, there was uncertainty as to the character of the initial CS state because both  $\text{P}_{\text{D2}}^{\delta+}\text{P}_{\text{D1}}^{\delta-}$  and  $\text{Chl}_{\text{D1}}^{\delta+}\text{Phe}_{\text{D1}}^{\delta-}$  gave reasonable fits to the data with the former yielding slightly better agreement to experimental data considered. It is important to note here that the experimental data was, however, entirely from electronic spectroscopies.

While uncertainty surrounds the involvement and extent of exciton-CT mixing in the PSII-RC, studies have suggested that the mixed CT states are responsible for the far-red excitation of PSII.<sup>36–38</sup> Although the absorption of the PSII-RC and the required redox potential of water oxidation were believed to be located below 690 nm, it was demonstrated that PSII can be operated by the far red light beyond 690 nm (exhibiting activities including oxygen evolution).<sup>36,39</sup> Additionally, recent EPR experimental<sup>37</sup> and QM/MM theoretical<sup>38</sup> studies suggest that the far-red light excitation of PSII involves a lower lying CT state with a hole localized on Chl<sub>D1</sub> rather than P<sub>D2</sub>. However, just as spectral congestion obscures the assignment of the initial electron acceptor, the character of these mixed CT states remains undetermined.

Compared to the previously mentioned techniques, the emerging method of two-dimensional electronic-vibrational (2DEV) spectroscopy, which correlates electronic excitation and mid-IR detection,<sup>40–44</sup> has the potential to overcome the challenges associated with congested electronic spectra. In particular, the simultaneous spectral resolution along both the visible excitation and IR detection axis has been shown to enable the clear assignment of transient species.<sup>41–44</sup> In this study, we investigated the excited state dynamics of the PSII-RC via 2DEV spectroscopy. Both highly excitation frequency-dependent spectral structure and dynamics were clearly resolved. This allowed for a broad analysis of the excitonic composition of the PSII-RC and direct insight into the involvement of mixed exciton-CT states found to be directly prepared upon photoexcitation. Further, the spectra facilitated an assignment of the initial electron acceptor and enabled the excitation energy transfer (EET) and electron transfer pathways initiated by peripheral antenna excitation or RC pigments excitation to be disentangled.

## 2 RESULTS AND DISCUSSION

**General insights from the 2DEV spectra and IR band assignments.** Figure 1b shows the 2DEV spectrum of the PSII-RC 170 fs after photoexcitation. Of note is the significant excitation frequency ( $\omega_{\text{exc.}}$ )-dependence of the vibrationally resolved structure along the detection axis ( $\omega_{\text{det.}}$ ) which, as we will demonstrate, allows for an excitonic state-specific analysis of the spectra with high frequency resolution (i.e. vibrationally resolved excitonic structure). For example, photoinduced absorptions (PIA) spanning  $\omega_{\text{det.}} = 1,710\text{-}1,760\text{ cm}^{-1}$  were seen to clearly favor the lower-lying excitonic states. Other strong indications of this  $\omega_{\text{exc.}}$ -dependent behavior were observed in the ground state bleach (GSB) region spanning  $\omega_{\text{det.}} = 1,680\text{-}1,710\text{ cm}^{-1}$  and the PIAs at  $\omega_{\text{det.}} = 1,620\text{-}1,670\text{ cm}^{-1}$ . These three regions are of particular interest because, here, vibrational modes belonging to both the neutral and ionic forms of Chl and Phe can be clearly distinguished—thus serving as sensitive markers for the EET and CT steps leading to CS as well as the character of the excitonic states.

The vibrational structure of the PSII-RC is not only highly  $\omega_{\text{exc.}}$ -dependent, but also shows a significant time-dependence. Therefore, our assignments will be based on the vibrational structure at specific  $\omega_{\text{exc.}}$  corresponding to the energies of exciton 2 ( $14,690\text{ cm}^{-1}$ ) and exciton 8 ( $14,940\text{ cm}^{-1}$ ) in the model by Novoderezhkin et al.,<sup>35</sup> which covers the relevant pigments along the D1 branch, and at either early or later waiting times (Figure 2).

Generally, the GSB observed at  $\omega_{\text{det.}} = 1,680\text{-}1,710\text{ cm}^{-1}$  is assigned to the keto CO stretching mode of Chl/Phe.<sup>29,31,32</sup> On the electronic ground state, the frequency of this keto mode depends on the polarity of the environment and the presence of hydrogen bonding from surrounding media (the larger the polarity, or the stronger the hydrogen bond, the lower the frequency of the keto mode). Thus, the GSB can be used to broadly distinguish pigment contributions (further discussed in the next section). For example, in Figure 2, it is apparent at early waiting times that the GSB band of exciton 8 shows much more signal amplitude at  $1,680\text{-}1,700\text{ cm}^{-1}$  compared to that of the exciton 2. This is in line with a light-induced FTIR difference spectroscopic study which reported that Chl<sub>z</sub> shows a GSB at  $1,684\text{ cm}^{-1}$ ,<sup>31</sup> whereas P and Phe exhibit higher and lower frequency GSBs at  $1,704\text{ cm}^{-1}$  and  $1,677\text{ cm}^{-1}$ , respectively.<sup>29,31,32</sup>

On the electronically excited state, the keto modes of Chl and Phe exhibit redshifted absorption.<sup>11,45</sup> For example, in THF, the keto stretching mode in the previously measured Chl\*/Chl difference spectrum was seen to shift from  $1,695\text{ cm}^{-1}$  to  $1,660\text{ cm}^{-1}$ .<sup>11</sup> Correspondingly, the negative signal at  $\omega_{\text{det.}} = 1,620\text{-}1,670\text{ cm}^{-1}$  in both exciton 2 and 8 is broadly assigned to the excited state absorption (ESA) of the keto modes of Chl and Phe. At later waiting times, however, there is a notable evolution in the vibrational structure of this region (Figure 2). Focusing on exciton 2, a clear dip at  $1,657\text{ cm}^{-1}$  appeared concomitantly with a new peak emerging at  $1,666\text{ cm}^{-1}$ . While both the P<sup>+</sup>/P and Phe<sup>-</sup>/Phe difference spectra exhibit features in this region at frequencies of  $1,653\text{-}1,655\text{ cm}^{-1}$  and  $1,659\text{ cm}^{-1}$ ,<sup>29,31,32</sup> respectively, the signal for Phe<sup>-</sup>/Phe agrees more closely with the observed feature at  $1,657\text{ cm}^{-1}$ . Resonance Raman spectroscopy of PSII-RC shows no signal at  $1640\text{-}1660\text{ cm}^{-1}$ , thus Groot et al. and Noguchi et al. suggest that the band at  $1657\text{ cm}^{-1}$  is assigned to the amide CO mode reflecting the CS at the RC, rather than keto stretching mode of Chl or Phe.<sup>11,31</sup> The band at  $1,666\text{ cm}^{-1}$  is similar to both Phe<sup>-</sup>/Phe and P<sup>+</sup>/P showing signal at  $1,662\text{ cm}^{-1}$  and  $1,663\text{ cm}^{-1}$ ,<sup>29,31,32</sup> respectively, which has been suggested as a counterpart of the previously mentioned band.<sup>31</sup> A more definitive assignment is reserved for later discussion.

This leaves the remaining PIA region spanning  $1,710\text{-}1,760\text{ cm}^{-1}$ . While the ester modes Chl\* and Phe\* fall in this region,<sup>11</sup> they are known to be very weak and would unlikely account for the full intensity of the observed features. Further, assuming that this region is only composed of Chl\* and Phe\* ester modes would not account for the significant  $\omega_{\text{exc.}}$ -dependence clearly present in Figure 1b. If this was the case, then this region should have a near uniform intensity across excitons 3 through 7 which have similar pigment contributions and exciton transition dipole strengths,<sup>35</sup> but this is clearly not so (Figure 1b). As a result, contributions from Chl\* and Phe\* ester modes are likely small, which should leave this a relatively clear spectral window, yet, strong features are apparent in the 2DEV spectra. The Phe<sup>-</sup>/Phe difference spectrum measured in PSII, however, shows characteristic signatures in this region, still related to the ester

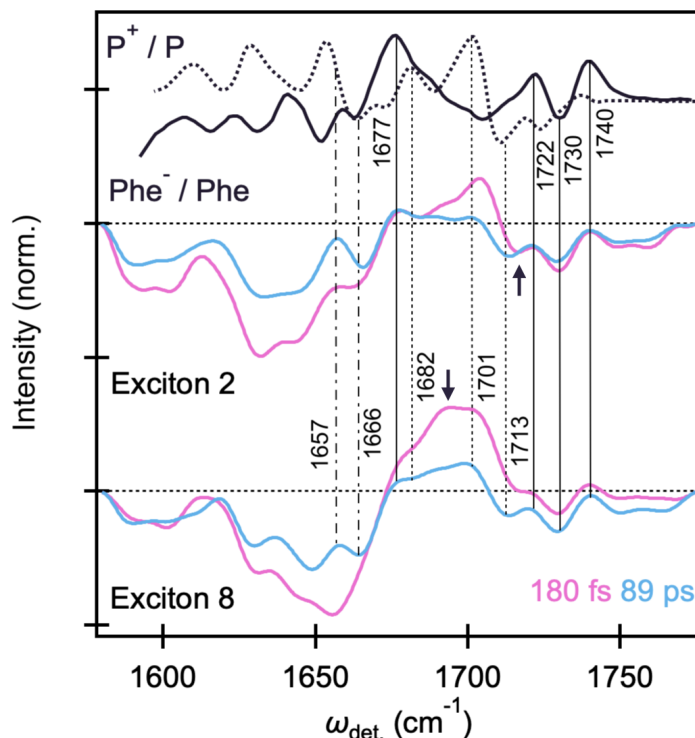


Figure 2: Exciton-specific vibrational structure and IR assignments. Slices of 2DEV spectrum at  $\omega_{\text{exc.}} = 14,690 \text{ cm}^{-1}$  and  $\omega_{\text{exc.}} = 14,940 \text{ cm}^{-1}$ , corresponding to the energies of exciton 2 and 8 at early (pink, 180 fs) and later (blue, 89 ps) waiting times. The difference absorption spectra of  $\text{P}^+/\text{P}$  (dotted line) and  $\text{Phe}^-/\text{Phe}$  (solid line) are shown above for comparison (where the signs have been reversed to match the convention of the 2DEV data). Vertical dotted (solid) lines indicate to band assignments corresponding  $\text{P}^+/\text{P}$  ( $\text{Phe}^-/\text{Phe}$ ) while dash-dotted lines distinguish more ambiguous assignments. The black arrow in exciton 2 marks the  $\text{Chl}_{\text{D1}}^+$  mode at  $1,716 \text{ cm}^{-1}$  and in exciton 8 marks the  $\text{Chl}_{\text{D1}}$  ground state bleach. The  $\text{P}^+/\text{P}$  and  $\text{Phe}^-/\text{Phe}$  spectra are reproduced from Ref. <sup>30</sup> and <sup>29</sup> with permission.

mode of chromophore itself or surrounding amino acid residue, with strong absorptions at  $1,722 \text{ cm}^{-1}$ ,  $1,730 \text{ cm}^{-1}$ , and  $1,739 \text{ cm}^{-1}$  (Figure 2).<sup>29,32</sup> The corresponding peaks in the 2DEV spectrum (at  $1,722 \text{ cm}^{-1}$ ,  $1,730 \text{ cm}^{-1}$ , and  $1,740 \text{ cm}^{-1}$ ), apparent at early waiting times for exciton 2 and emerging later for exciton 8, are therefore assigned to  $\text{Phe}^-$ . It should be noted that exciton 8 does show a slight negative signal around  $1,730 \text{ cm}^{-1}$  immediately after photoexcitation, despite being near fully characterized by  $\text{Chl}_{\text{D1}}$ . We attribute this signal to either slight contributions from the ester ESA, some degree of overlap between excitonic bands as these slices only represent the zero phonon transitions and the actual absorption has finite bandwidth. The ester mode of the  $\text{Chl } a$  cation (in THF), on the other hand, is known to blueshift from  $1,738 \text{ cm}^{-1}$  (neutral) to  $1,750 \text{ cm}^{-1}$ .<sup>29</sup> Yet, the  $\text{P}^+/\text{P}$  difference spectrum (Figure 2) does not exhibit any corresponding characteristic absorptions in this region (the ester mode of  $\text{P}^+$  appears at  $1,743 \text{ cm}^{-1}$ ).<sup>30</sup> Thus, the bands in this region,  $1,750 \text{ cm}^{-1}$  and  $1,764 \text{ cm}^{-1}$ , are related to the intermediate  $\text{Chl}$  cation ( $\text{Chl}_{\text{D1}}^+$ ) which are also clearly present in the structure of exciton 2 at early waiting times.

Further characteristic of the  $\text{Chl } a$  cation is a significantly blueshifted keto stretch, to  $1,718 \text{ cm}^{-1}$ , (on the order of  $25 \text{ cm}^{-1}$ ) versus neutral  $\text{Chl } a$  in THF.<sup>33</sup> At early waiting times in exciton 2, for example, a peak is observed at  $1,716 \text{ cm}^{-1}$  which we assign to  $\text{Chl}_{\text{D1}}^+$ . However, at later waiting times, this peak noticeably redshifts to  $1,713 \text{ cm}^{-1}$ , towards agreement with the characteristic  $\text{P}^+$  absorption at  $1,711 \text{ cm}^{-1}$ . This dynamical behavior will be the focus of later discussion.

To summarize, the significant markers tracking CS in this study are as follows:  $\text{Phe}^-$  ( $1,722 \text{ cm}^{-1}$ ,  $1,730 \text{ cm}^{-1}$ , and  $1,740 \text{ cm}^{-1}$ ),  $\text{Chl}_{\text{D1}}^+$  (at early waiting times:  $1,716 \text{ cm}^{-1}$ ,  $1,750 \text{ cm}^{-1}$ , and  $1,764 \text{ cm}^{-1}$ ), and  $\text{P}^+$  (at later waiting times:  $1,713 \text{ cm}^{-1}$ ). The GSB of the amide CO bands at  $1,657 \text{ cm}^{-1}$  and its up-shifted counterpart at  $1,666 \text{ cm}^{-1}$  reflecting the CS at RC, where the former likely has predominant contributions from  $\text{Phe}^-$ , while the latter could potentially be a mixture of  $\text{Phe}^-$  and  $\text{P}^+$ .

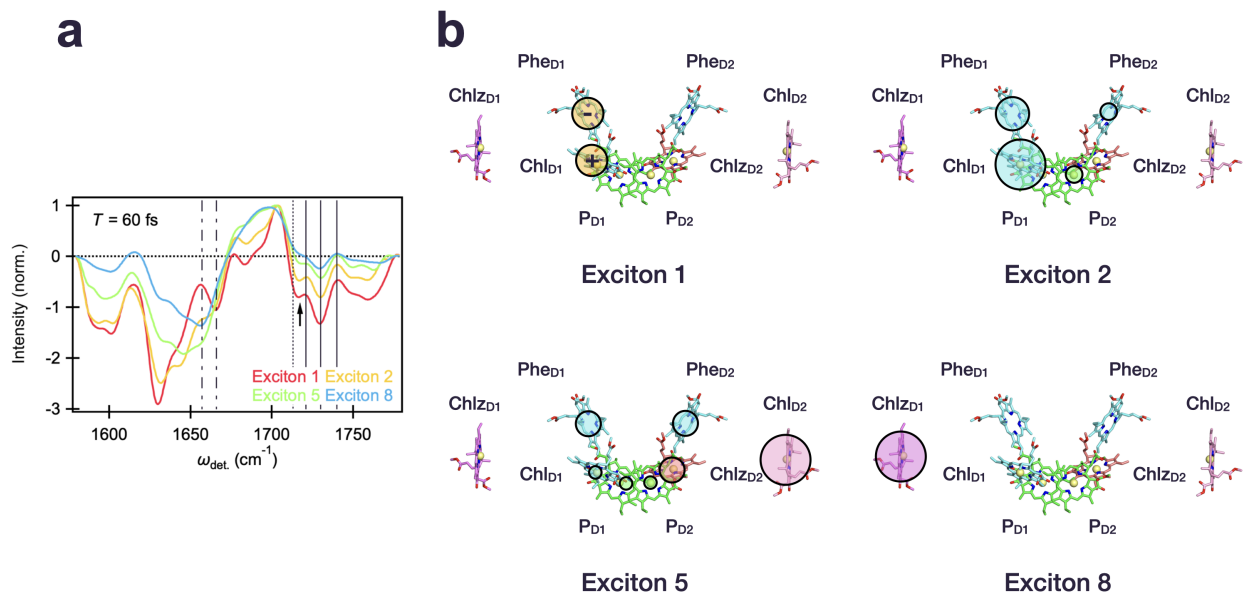


Figure 3: Assignment of excitonic composition and charge transfer character. (a) Slice along  $\omega_{det.}$  of the 2DEV spectrum corresponding to exciton 1 (red, integrated at  $\omega_{exc.} = 14,500\text{-}14,650\text{ cm}^{-1}$ ), exciton 2 (yellow,  $\omega_{exc.} = 14,690\text{ cm}^{-1}$ ), exciton 5 (green,  $\omega_{exc.} = 14,850\text{ cm}^{-1}$ ), and exciton 8 (blue,  $\omega_{exc.} = 14,940\text{ cm}^{-1}$ ) at a waiting time of 60 fs. The vertical solid, dotted, and dash-dotted lines, as well as the black arrow follow the same convention as in Figure 2. (b) Character of initial charge transfer state, exciton 1, along with the site contributions of excitons 2, 5, and 8 where the area of the shaded circles is proportional to the population of the corresponding sites based on the model of Novoderezhkin et al.<sup>35</sup> For clarity, the slight, additional contributions from D1 pigments, nearly identical to the relative contributions of exciton 2, were omitted from exciton 1. Likewise, the charge transfer character present in excitons 2 and 5 was precluded for simplicity.

**Excitonic composition and charge transfer character.** Following the vibrational assignments, we focus on a comparison of the vibrational structure at specific excitonic energies based on the model by Novoderezhkin et al.,<sup>35</sup> in order to understand the character of the excitonic states and degree of CT mixing. Figure 3a shows the vibrational structure corresponding to exciton 1, 2, 5, and 8 at an early waiting time. We note again that the exciton energies discussed thus far are zero phonon lines (shown in Figure 1b). However, it has been reported that the actual absorption of the CT state shows a significant blue shift ( $\sim 5\text{ nm}$ ) as a result of coupling to low-frequency phonons in the environment, compared to other excitonic bands ( $1\text{-}2\text{ nm}$ ).<sup>35</sup> Thus, to investigate the CT state specifically, the 2DEV signal corresponding to exciton 1 as shown in Figure 3a was integrated in the range  $\omega_{exc} = 14,500\text{-}14,650\text{ cm}^{-1}$ .

At early time, the exciton 1 signal, formed directly upon photoexcitation, shows clear structure corresponding to Phe<sup>-</sup> ( $1,722\text{ cm}^{-1}$ ,  $1,730\text{ cm}^{-1}$ , and  $1,740\text{ cm}^{-1}$ ), Chl<sub>D1</sub><sup>+</sup> ( $1,716\text{ cm}^{-1}$ ,  $1,750\text{ cm}^{-1}$ , and  $1,764\text{ cm}^{-1}$ ). In addition, the amide CO bands reflecting CS at  $1,657\text{ cm}^{-1}$  and  $1,666\text{ cm}^{-1}$  show clear structure compared on the other excitonic states, highlighting the significant CT character of exciton 1 state. The characteristic P<sup>+</sup> signal ( $1,713\text{ cm}^{-1}$ ) only appears at later waiting times and is accompanied by evolution at both of the aforementioned band positions as well as a decay in the  $1,750\text{ cm}^{-1}$  region assigned to Chl<sub>D1</sub><sup>+</sup> (Figure S1)—collectively indicating a conspicuous lack of initial contributions from P<sup>+</sup>.

The lack of P<sup>+</sup> is in contrast to several previous spectroscopic studies that suggested there are two CS pathways in the PSII-RC.<sup>21,22,24,34</sup> However, these experiments utilized spectroscopic methods solely in the visible region which are significantly disadvantaged when it comes to untangling the highly overlapping signals of the relevant states. In this case, the vibrational characterization of exciton 1 afforded by the application of 2DEV spectroscopy provides direct evidence that the initial CT state in the PSII-RC is characterized by Chl<sub>D1</sub><sup>+</sup>Phe<sup>-</sup> rather than P<sub>D2</sub><sup>+</sup>P<sub>D1</sub><sup>-</sup> (Figure 3b). Such a result is consistent with a recent QM/MM calculation, utilizing range-separated TD-DFT theory and the coupled cluster theory with single and double excitations (CCSD), which proposed that the lowest CT state was Chl<sub>D1</sub><sup>+</sup>Phe<sup>-</sup>.<sup>38</sup> A previous transient IR study also suggested that the initial electron acceptor is Phe,<sup>11</sup> however, this study relied on an

extrinsic deconvolution of the vibrational spectrum as opposed to the intrinsic ability of 2DEV spectroscopy to separate excitonic and CT contributions along the  $\omega_{\text{exc}}$  dimension. This advantage of 2DEV spectroscopy is particularly useful in the characterization of the CT state which is only weakly optically allowed and can therefore be easily obscured in other spectroscopic methods.

Considering the other states, an analysis of the GSB features of exciton 2 and 8 characterize these excitons as predominantly composed of RC pigments in the active (D1) branch and of the peripheral  $\text{Chl}_{\text{D1}}$ , respectively, which is consistent with the model put forth by Novoderezhkin et al. (Figure 3b).<sup>35</sup> These assignments also substantiate that Chl and Phe at different binding position in the PSII-RC are indeed excited by different excitation frequencies—offering support for the importance of the protein environment in tuning the site energies of the embedded pigments.<sup>38</sup>

Exciton 2 also notably displays characteristic  $\text{Chl}_{\text{D1}}^+$  and  $\text{Phe}^-$  signals at early waiting times (Figure 3a). In comparison to exciton 5, which is mainly composed of RC pigments in addition to  $\text{Chl}_{\text{D2}}$  (Figure 3b), these CT signatures in exciton 2 are markedly more pronounced. Here, we have chosen exciton 5 as a representative for the energetically intermediate excitonic states, where there is congestion even in the 2DEV spectra. However, the vibrational structure is still telling in that the additional  $\text{Chl}_{\text{D2}}$  contributions of exciton 5 should be similar to those of  $\text{Chl}_{\text{D1}}$ , which is indeed reflected in the fact that exciton 5 resembles a mixture of exciton 2 (mainly RC pigments) and exciton 8 (mainly composed of a peripheral pigment). This comparison highlights the enhanced CT character in exciton 2 versus exciton 5 at early waiting times which confirms the suggestion put forth in the model by Novoderezhkin et al.<sup>35</sup> that exciton 2 is responsible for initiating primary charge separation. Further, in the model, exciton 1 was taken to be characterized by a CT state which borrowed intensity from the neighboring state, exciton 2. This is in agreement with the close resemblance between the GSB and ESA (particularly below  $1650\text{ cm}^{-1}$  which is outside of the dominant window for the CS markers) structure of exciton 1 compared to that of exciton 2 (Figure 3a) and signifies similar overall pigment contributions. This point is made even clearer on comparison of exciton 1 versus exciton 5 or 8 where there is little similarity in these regions. Correspondingly, this indicates that exciton 2 is characterized by a mixed exciton-CT state, rather than a purely excitonic state that rapidly evolves to the CT state. The mixed character between exciton 1 and 2 also offers a mechanism through which rapid charge separation can be initiated in the RC.

**Charge separation dynamics.** To elucidate the dynamics, a global analysis of the data with sequential modeling was performed. We note that while the time constants represent a convolution of various processes, this method is able to holistically capture the spectral evolution along both frequency dimensions. Therefore, the analysis captures the  $\omega_{\text{exc}}$ -dependent spectra and dynamics, the latter which can be largely disentangled via vibrational signatures as we will show. The two-dimensional-evolution associated difference spectra (2D-EADS) analysis (Figure S1), which can be thought as the two-dimensional analogue of EADS,<sup>46</sup> required five components for a reasonable fit (170 fs, 660 fs, 8.2 ps, 17 ps, and a non-decaying offset component beyond 100 ps, the duration of the experiment).

Figure 4 contains exciton-specific slices through the actual 2DEV spectra along  $\omega_{\text{det}}$  at the earliest resolvable waiting time and at subsequent waiting times corresponding to each of the above mentioned time constants. Throughout, we focus our attention on excitons 2, 5, and 8 as these states have substantially more oscillator strength than exciton 1 and therefore will have a larger influence on the obtained time constants. The evolution associated with these time constants can be interpreted such that each spectrum (or slice) evolves into the next one with the associated time constant. For example, in exciton 2 (Figure 4b), spectral evolution on the 170 fs timescale can be understood through a comparison of the pink and yellow slices. Noticeably, there is growth at  $1,657\text{ cm}^{-1}$ , a characteristic marker for CS. However, in exciton 5 and 8 (Figure 4c and d, respectively) there is no such growth indicative of CS, rather there are only slight changes in the keto GSB and ESA regions. On the 660 fs timescale (comparison of the yellow and green slices in Figure 4b), exciton 2 exhibits further growth at  $1,657\text{ cm}^{-1}$  and  $1,666\text{ cm}^{-1}$  while a slight shoulder begins to emerge in this region for exciton 5. This evolution is also accompanied by marked changes in the keto ESA structure. We assign both the 170 fs and 660 fs timescales to progressive completion of CS, i.e.  $(\text{Chl}_{\text{D1}}^{\delta+}\text{Phe}^{\delta-})^* \rightarrow \text{Chl}_{\text{D1}}^+\text{Phe}^-$  (more pronounced for exciton 2), convoluted with EET within the excitonic manifold (more pronounced for exciton 5) and an environmental response. These timescales also agree with previous works which suggested that there is a fast component to the EET dynamics (100-200 fs time scale)<sup>12</sup> and that initial CS occurs within 600-800 fs,<sup>11</sup> among others which have reported multiexponential CS dynamics.<sup>21,24</sup> The distinction here is that the vibrational structure allows for a targeted assessment of the dynamical components for each of the states.

On an 8.2 ps timescale, both the  $1,657\text{ cm}^{-1}$  and  $1,666\text{ cm}^{-1}$  CS markers exhibit further evolution along with a distinct, progressive redshift in the band at  $1,716\text{ cm}^{-1}$  to  $1,713\text{ cm}^{-1}$  for excitons 1, 2, and 5. This component is similar to the previously reported timescale for  $\text{Chl}_{\text{D1}}^+\text{Phe}^- \rightarrow \text{P}^+\text{Phe}^-$  of 6 ps.<sup>11</sup> Additionally, in a previous light-induced FTIR difference spectroscopic study, it was proposed that the blue shift of the keto stretch of Chl cation is smaller for the charge delocalized dimeric Chl ( $\sim 10\text{ cm}^{-1}$  in the case of P680<sup>+</sup>) compared to that of monomeric Chl ( $\sim 30\text{ cm}^{-1}$ ).<sup>47</sup> Both experimental<sup>47,48</sup> and theoretical<sup>49,50</sup> efforts further support that the P680 cation is partially delocalized over the  $\text{P}_{\text{D1}}$  and  $\text{P}_{\text{D2}}$  pigments. Thus, we assign the slight red shift as the hole migration towards a more delocalized cationic state,

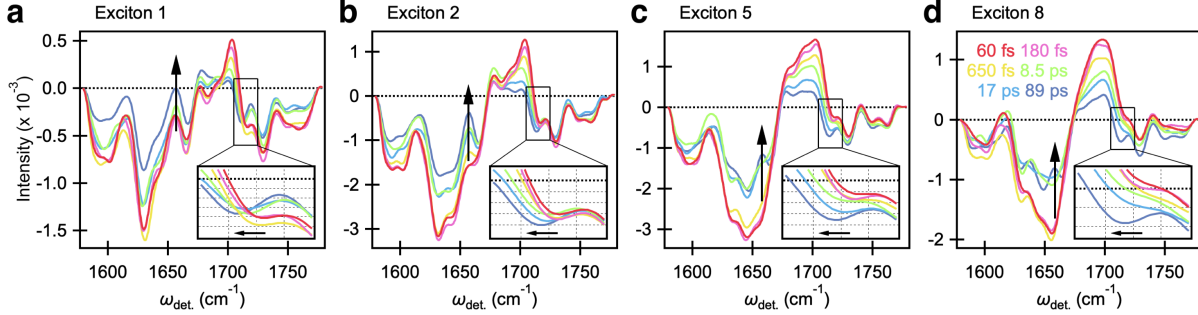


Figure 4: Dynamics of the PSII-RC. The time-dependent evolution of 2DEV spectra corresponding to excitons 1, 2, 5, and 8. Inset shows the range of  $\omega_{\text{det}} = 1705\text{-}1725 \text{ cm}^{-1}$ , highlighting the red-shifting behavior of the  $\text{Chl}^+$  band.

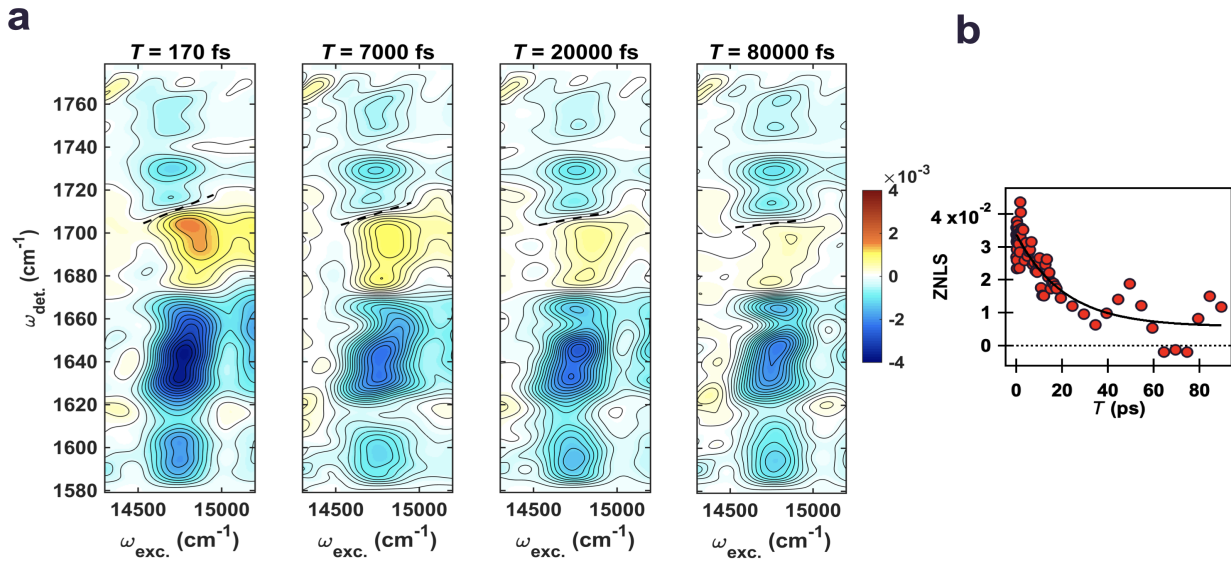


Figure 5: 2DEV spectral evolution and ZNLS dynamics of the PSII-RC. (a) 2DEV spectra of the PSII-RC at different waiting times. Zero node line slope (ZNLS), obtained by a linear fit of the zero signal intensity distribution along the excitation axis, is depicted in the spectra as a dotted line. Contour levels are drawn in 5% intervals. (b) ZNLS dynamics of the PSII-RC. Red dots indicate the ZNLS value at each waiting time and the black curve shows the fit result of a single exponential function (and an offset) with a time constant of  $21 \pm 4 \text{ ps}$ .

i.e.  $\text{Chl}_{\text{D1}}^+\text{Phe}^- \rightarrow (\text{P}_{\text{D1}}\text{P}_{\text{D2}})^+\text{Phe}^-$  (likely in addition to further environmental response to CS). Considering that the mode at  $1,713 \text{ cm}^{-1}$ , the characteristic marker for  $\text{P}^+$ , only appears on an  $8.2 \text{ ps}$  timescale, it is very unlikely that  $\text{P}^+$  contributes appreciably to the features at  $1,657 \text{ cm}^{-1}$  and  $1,666 \text{ cm}^{-1}$  at earlier waiting times. The evolution observed around  $1,657 \text{ cm}^{-1}$  and  $1,666 \text{ cm}^{-1}$  at later waiting times can therefore be understood as arising from both  $\text{Phe}^-$  and  $\text{P}^+$ .

The final  $17 \text{ ps}$  component can be understood as predominantly reflecting CS limited by EET from peripheral Chlz to RC pigments as only significant evolution at the CS markers is observed on this timescale for exciton 8 (Figure 4d). This timescale is also captured by the zero node line slope (ZNLS) present at  $\omega_{\text{det}} = 1,710 \text{ cm}^{-1}$  (Figure 5a, dotted line) in the spectra which decays with a time constant of  $21 \pm 4 \text{ ps}$  (Figure 5b) and grossly indicates equilibration within the excitonic manifold. We note that while the ZNLS trends toward zero, a non-decaying component beyond the duration of the experiment ( $>100 \text{ ps}$ ) suggests the presence of the inhomogeneous CS due to the different conformational distributions of the proteins on the ground state.<sup>21</sup> This timescale also falls within the previously established range ( $14 \text{ ps}$  to  $37 \text{ ps}$  determined at temperatures of  $77 \text{ K}$  and  $277 \text{ K}$ , respectively) for EET from peripheral Chlz to RC pigments.<sup>13,19</sup>

**Concluding comments.** Our results demonstrate that the CT state can be prepared directly upon photoexcitation, which is characterized by  $\text{Chl}_{\text{D1}}^{\delta'+} \text{Phe}^{\delta'-}$  ( $\delta' > \delta$ ), and indicate that CS is facilitated by exciton-CT mixing with a contribution from  $(\text{Chl}_{\text{D1}}^{\delta'+} \text{Phe}^{\delta'-})^*$  throughout the excitonic manifold. The data further establishes that the initial electron acceptor in the PSII-RC is Phe with no appreciable competition from  $\text{P}_{\text{D1}}$ —independent of excitation wavelength. These results are entirely in agreement with the recent theoretical work of Sirohiwal et al. where the  $\text{Chl}_{\text{D1}}^+ \text{Phe}^-$  CT state was found to be the lowest energy excitation globally within the PSII-RC.<sup>38</sup> Further, no similarly low energy CT states involving  $\text{P}_{\text{D1}}\text{P}_{\text{D2}}$  were found,<sup>38</sup> thus theoretically excluding the special pair as a candidate for initial CS as our experimental data supports. This is notably distinct from the bacterial RC where CS is largely initiated at the special pair (P) with the A branch bacteriochlorophyll (BChl) acting as the primary acceptor. The distinct excitation asymmetry in the PSII-RC has been rationalized as a direct consequence of the electrostatic effect of the protein environment which likely arose as an evolutionary accommodation of water splitting in oxygenic photosynthetic systems (particularly its operation in the far-red).<sup>36–38</sup> However, this remains an open question as the initial CS step itself in the has long evaded clear characterization.

## ACKNOWLEDGMENTS

We thank Rafael Picorel for advice regarding isolation of the PSII-RC. This research was supported by the U.S. Department of Energy, Office of Science, Basic Energy Sciences, Chemical Sciences, Geosciences, and Biosciences Division. Y.Y. appreciates the support of the Japan Society for the Promotion of Science (JSPS) Postdoctoral Fellowship for Research Abroad. E.A.A. acknowledges the support of the National Science Foundation Graduate Research Fellowship (Grant No. DGE 1752814).

## REFERENCES

1. Wydrzynski, T. J., Satoh, K. & Freeman, J. A. *Photosystem II The Light-Driven Water:Plastoquinone Oxidoreductase*. vol. 22 (Springer Netherlands, 2005).
2. Blankenship, R. E. *Molecular Mechanisms of Photosynthesis, 2nd Edition*. (Wiley, 2014).
3. Shen, J.-R. The Structure of Photosystem II and the Mechanism of Water Oxidation in Photosynthesis. *Annu. Rev. Plant Biol.* **66**, 23–48 (2015).
4. Renger, G. & Renger, T. Photosystem II: The machinery of photosynthetic water splitting. *Photosynth. Res.* **98**, 53–80 (2008).
5. Croce, R. & Van Amerongen, H. Light-harvesting and structural organization of Photosystem II: From individual complexes to thylakoid membrane. *J. Photochem. Photobiol. B Biol.* **104**, 142–153 (2011).
6. Romero, E., Novoderezhkin, V. I. & Van Grondelle, R. Quantum design of photosynthesis for bio-inspired solar-energy conversion. *Nature* **543**, 355–365 (2017).
7. Loll, B., Kern, J., Saenger, W., Zouni, A. & Biesiadka, J. Towards complete cofactor arrangement in the 3.0 Å resolution structure of photosystem II. *Nature* **438**, 1040–1044 (2005).
8. Umena, Y., Kawakami, K., Shen, J.-R. R. & Kamiya, N. Crystal structure of oxygen-evolving photosystem II at a resolution of 1.9Å. *Nature* **473**, 55–60 (2011).
9. Shelaev, I. V. *et al.* Primary light-energy conversion in tetrameric chlorophyll structure of photosystem II and bacterial reaction centers: II. Femto- and picosecond charge separation in PSII D1/D2/Cyt b559 complex. *Photosynth. Res.* **98**, 95–103 (2008).
10. Nadtochenko, V. A., Semenov, A. Y. & Shuvalov, V. A. Formation and decay of P680 (PD1-PD2) +PheD1- radical ion pair in photosystem II core complexes. *Biochim. Biophys. Acta - Bioenerg.* **1837**, 1384–1388 (2014).
11. Groot, M. L. *et al.* Initial electron donor and acceptor in isolated Photosystem II reaction centers identified with femtosecond mid-IR spectroscopy. *Proc. Natl. Acad. Sci.* **102**, 13087–13092 (2005).
12. Prokhorenko, V. I. & Holzwarth, A. R. Primary processes and structure of the photosystem II reaction center: A photon echo study. *J. Phys. Chem. B* **104**, 11563–11578 (2000).
13. Holzwarth, A. R. *et al.* Kinetics and mechanism of electron transfer in intact photosystem II and in the isolated reaction center: Pheophytin is the primary electron acceptor. *Proc. Natl. Acad. Sci.* **103**, 6895–6900 (2006).
14. Myers, J. A. *et al.* Two-Dimensional Electronic Spectroscopy of the D1-D2-cyt b559 Photosystem II Reaction Center Complex. *J. Phys. Chem. Lett.* **1**, 2774–2780 (2010).
15. Durrant, J. R. *et al.* A multimer model for P680, the primary electron donor of photosystem II. *Proc. Natl. Acad. Sci. U. S. A.* **92**, 4798–4802 (1995).



16. Raszewski, G., Diner, B. A., Schlodder, E. & Renger, T. Spectroscopic properties of reaction center pigments in photosystem II core complexes: Revision of the multimer model. *Biophys. J.* **95**, 105–119 (2008).
17. Crystall, B. *et al.* Observation of Multiple Radical Pair States in Photosystem 2 Reaction Centers. *Biochemistry* **30**, 7573–7586 (1991).
18. Konermann, L., Gatzen, G. & Holzwarth, A. R. Primary processes and structure of the photosystem II reaction center. 5. Modeling of the fluorescence kinetics of the D1-D2-cyt-b559 complex at 77 K. *J. Phys. Chem. B* **101**, 2933–2944 (1997).
19. Visser, H. M. *et al.* Subpicosecond transient absorption difference spectroscopy on the reaction center of photosystem II: Radical pair formation at 77 K. *J. Phys. Chem.* **99**, 15304–15309 (1995).
20. Groot, M. L. *et al.* Charge separation in the reaction center of photosystem II studied as a function of temperature. *Proc. Natl. Acad. Sci. U. S. A.* **94**, 4389–4394 (1997).
21. Romero, E., Van Stokkum, I. H. M., Novoderezhkin, V. I., Dekker, J. P. & Van Grondelle, R. Two different charge separation pathways in photosystem II. *Biochemistry* **49**, 4300–4307 (2010).
22. Romero, E. *et al.* Quantum coherence in photosynthesis for efficient solar-energy conversion. *Nat. Phys.* **10**, 676–682 (2014).
23. Fuller, F. D. *et al.* Vibronic coherence in oxygenic photosynthesis. *Nat. Chem.* **6**, 706–711 (2014).
24. Duan, H.-G. *et al.* Primary Charge Separation in the Photosystem II Reaction Center Revealed by a Global Analysis of the Two-dimensional Electronic Spectra. *Sci. Rep.* **7**, 12347 (2017).
25. Groot, M. L., Van Wilderen, L. J. G. W. & Di Donato, M. Time-resolved methods in biophysics. 5. Femtosecond time-resolved and dispersed infrared spectroscopy on proteins. *Photochem. Photobiol. Sci.* **6**, 501–507 (2007).
26. Di Donato, M. & Groot, M. L. Ultrafast infrared spectroscopy in photosynthesis. *Biochim. Biophys. Acta - Bioenerg.* **1847**, 2–11 (2015).
27. Breton, J. Fourier transform infrared spectroscopy of primary electron donors in type I photosynthetic reaction centers. *Biochim. Biophys. Acta - Bioenerg.* **1507**, 180–193 (2001).
28. Noguchi, T. & Berthomieu, C. Molecular Analysis by Vibrational Spectroscopy. in *Photosystem II: The Light-Driven Water:Plastoquinone Oxidoreductase* (eds. Wydrzynski, T. J., Satoh, K. & Freeman, J. A.) 367–387 (Springer Netherlands, 2005). doi:10.1007/1-4020-4254-X\_17.
29. Nabedryk, E. *et al.* Characterization of bonding interactions of the intermediary electron acceptor in the reaction center of Photosystem II by FTIR spectroscopy. *Biochim. Biophys. Acta - Bioenerg.* **1016**, 49–54 (1990).
30. Breton, J., Hienerwadel, R. & Nabedryk, E. FTIR Difference Spectrum of the Photooxidation of the Primary Electron Donor of Photosystem II. in *Spectroscopy of Biological Molecules: Modern Trends* 101–102 (Springer Netherlands, 1997). doi:10.1007/978-94-011-5622-6\_44.
31. Noguchi, T., Tomo, T. & Inoue, Y. Fourier transform infrared study of the cation radical of P680 in the photosystem II reaction center: Evidence for charge delocalization on the chlorophyll dimer. *Biochemistry* **37**, 13614–13625 (1998).
32. Noguchi, T., Tomo, T. & Kato, C. Triplet formation on a monomeric chlorophyll in the photosystem II reaction center as studied by time-resolved infrared spectroscopy. *Biochemistry* **40**, 2176–2185 (2001).
33. Nabedryk, E., Leonhard, M., Mäntele, W. & Breton, J. Fourier Transform Infrared Difference Spectroscopy Shows No Evidence for an Enolization of Chlorophyll a upon Cation Formation either in Vitro or during P700 Photooxidation. *Biochemistry* **29**, 3242–3247 (1990).
34. Romero, E. *et al.* Mixed exciton-charge-transfer states in photosystem II: Stark spectroscopy on site-directed mutants. *Biophys. J.* **103**, 185–194 (2012).
35. Novoderezhkin, V. I., Dekker, J. P. & van Grondelle, R. Mixing of Exciton and Charge-Transfer States in Photosystem II Reaction Centers: Modeling of Stark Spectra with Modified Redfield Theory. *Biophys. J.* **93**, 1293–1311 (2007).
36. Thapper, A., Mamedov, F., Mokvist, F., Hammarström, L. & Styring, S. Defining the far-red limit of photosystem II in Spinach. *Plant Cell* **21**, 2391–2401 (2009).
37. Pavlou, A., Jacques, J., Ahmadova, N., Mamedov, F. & Styring, S. The wavelength of the incident light determines the primary charge separation pathway in Photosystem II. *Sci. Rep.* **8**, 1–11 (2018).

38. Sirohiwal, A., Neese, F. & Pantazis, D. A. Protein Matrix Control of Reaction Center Excitation in Photosystem II. *J. Am. Chem. Soc.* **142**, 18174–18190 (2020).
39. Pettai, H., Oja, V., Freiberg, A. & Laisk, A. Photosynthetic activity of far-red light in green plants. *Biochim. Biophys. Acta - Bioenerg.* **1708**, 311–321 (2005).
40. Oliver, T. A. A., Lewis, N. H. C. & Fleming, G. R. Correlating the motion of electrons and nuclei with two-dimensional electronic-vibrational spectroscopy. *Proc. Natl. Acad. Sci.* **111**, 10061–10066 (2014).
41. Lewis, N. H. C. *et al.* Observation of Electronic Excitation Transfer Through Light Harvesting Complex II Using Two-Dimensional Electronic–Vibrational Spectroscopy. *J. Phys. Chem. Lett.* **7**, 4197–4206 (2016).
42. Arsenault, E. A. *et al.* Vibronic mixing enables ultrafast energy flow in light-harvesting complex II. *Nat. Commun.* **11**, 1460 (2020).
43. Arsenault, E. A., Yoneda, Y., Iwai, M., Niyogi, K. K. & Fleming, G. R. The role of mixed vibronic Qy-Qx states in green light absorption of light-harvesting complex II. *Nat. Commun.* **11**, 6011 (2020).
44. Yoneda, Y. *et al.* Electron–Nuclear Dynamics Accompanying Proton-Coupled Electron Transfer. *J. Am. Chem. Soc.* **143**, 3104–3112 (2021).
45. Groot, M. L., Breton, J., Van Wilderen, L. J. G. W., Dekker, J. P. & Van Grondelle, R. Femtosecond visible/visible and visible/mid-IR pump-probe study of the photosystem II core antenna complex CP47. *J. Phys. Chem. B* **108**, 8001–8006 (2004).
46. Van Stokkum, I. H. M., Larsen, D. S. & Van Grondelle, R. Global and target analysis of time-resolved spectra. *Biochim. Biophys. Acta - Bioenerg.* **1657**, 82–104 (2004).
47. Okubo, T., Tomo, T., Sugiura, M. & Noguchi, T. Perturbation of the structure of P680 and the charge distribution on its radical cation in isolated reaction center complexes of photosystem II as revealed by fourier transform infrared spectroscopy. *Biochemistry* **46**, 4390–4397 (2007).
48. Diner, B. A. *et al.* Site-directed mutations at D1-His198 and D2-His197 of photosystem II in *Synechocystis* PCC 6803: Sites of primary charge separation and cation and triplet stabilization. *Biochemistry* **40**, 9265–9281 (2001).
49. Saito, K. *et al.* Distribution of the cationic state over the chlorophyll pair of the photosystem II reaction center. *J. Am. Chem. Soc.* **133**, 14379–14388 (2011).
50. Narzi, D., Bovi, D., De Gaetano, P. & Guidoni, L. Dynamics of the Special Pair of Chlorophylls of Photosystem II. *J. Am. Chem. Soc.* **138**, 257–264 (2016).

#### Author contributions

Y.Y. and G.R.F. conceived the research. Y.Y., E.A.A., and K.O. performed the 2DEV experiments. Y.Y. analyzed the experimental data. M.I. prepared the sample. Y.Y., E.A.A., and G.R.F. wrote the manuscript. All authors discussed the results and contributed to the manuscript.

#### Competing financial interests

The authors declare no competing financial interests.

## Supplementary Information

# The initial charge separation step in oxygenic photosynthesis

*Yusuke Yoneda,<sup>1,2,5</sup> Eric A. Arsenault,<sup>1,2,3</sup> Kaydren Orcutt,<sup>1</sup> Masakazu Iwai<sup>2,4</sup> and Graham R.*

*Fleming<sup>1,2,3\*</sup>*

*<sup>1</sup>Department of Chemistry, University of California, Berkeley, CA 94720, USA*

*<sup>2</sup>Molecular Biophysics and Integrated Bioimaging Division, Lawrence Berkeley National*

*Laboratory, Berkeley, CA 94720, USA*

*<sup>3</sup>Kavli Energy Nanoscience Institute at Berkeley, Berkeley, CA 94720, USA*

*<sup>4</sup>Department of Plant and Microbial Biology, University of California, Berkeley, CA 94720,*

*USA*

*<sup>5</sup>Present Address: Research Center of Integrative Molecular Systems, Institute for Molecular*

*Science, National Institute of Natural Sciences, Okazaki, Aichi, 444-8585, Japan*

*\*grfleming@lbl.gov*

## Experimental Methods

**Two-dimensional electronic-vibrational spectroscopy.** A detailed description for the experimental setup of two-dimensional electronic-vibrational (2DEV) spectroscopy can be found elsewhere.<sup>1</sup> Briefly, the output of a Ti:sapphire oscillator (Vitara-S, Coherent) was regeneratively amplified with a 1 kHz repetition rate (Legend Elite, Coherent), an energy of 1 mJ/pulse and a pulse duration of 40 fs. The amplified pulse was divided into two and one was used to pump a home-built visible non-collinear optical parametric amplifier (NOPA). The other pulse was used to generate a mid-IR probe pulse (centered at 5.9  $\mu\text{m}$ ) by difference frequency generation with signal and idler pulses from a near-IR collinear OPA. The output of the NOPA (centered at 675 nm, 60 nm fwhm) was compressed to 20 fs at the sample position using a pair of prisms and an acousto-optic dispersive programmable filter (AODPF, Dazzler, Fastlite). The pulse pair was introduced to a retroreflector on a motorized translation stage to control the waiting time,  $T$ , between the pump and probe pulses. The total power of the pump pulses was set at 80 nJ and the pulses were focused into the sample with spot size of 250  $\mu\text{m}$ . The mid-IR pulse was divided by a 50:50 beam splitter to form probe and reference beams. The probe and reference beams were dispersed by a spectrometer (Horiba, Triax 180) and detected by a 64-pixel HgCdTe dual array (Infrared Systems Development). The cross-correlation

between visible and mid-IR pulses was estimated to be 130 fs by a step-like transient IR response of a 50  $\mu\text{m}$  Ge plate.

For each waiting time, a 2DEV spectrum was acquired by using the AODPF to scan the  $t_1$  delay over 0-100 fs with 2.5 fs steps. For each  $t_1$  delay, the signal was acquired with the relative phase between the pump pulses  $\varphi_{12}$  set by 0,  $2\pi/3$  and  $4\pi/3$ , and the desired signal was isolated by a  $3\times 1\times 1$  phase cycling scheme.<sup>2,3</sup> The excitation axis was obtained by a Fourier transformation over  $t_1$ . The signal was collected in the fully rotated frame with respect to  $t_1$ . For 2D-EADS analysis, the detection range was selected to be  $\omega_{\text{det.}} = 1620\text{-}1740\text{ cm}^{-1}$  because the dynamics in this range most fully reflects CS.

**Sample preparation.** All procedures for sample preparation were performed in the dark to minimize exposure to light as much as possible. We first isolated PSII-enriched membranes according to the previous literature with some modifications as follows.<sup>4,5</sup> We obtained spinach leaves (*Spinacia oleracea*) from a local store and kept in the dark overnight at 4 °C. The spinach leaves were briefly ground using a Waring blender in a buffer containing 50 mM MES-NaOH (pH 6.0), 400 mM NaCl, and 2 mM  $\text{MgCl}_2$  at 4 °C. The ground tissues were filtered through 4 layers of Miracloth (Millipore), and the filtered homogenate was centrifuged at  $1,400 \times g$  for 10 min at 4 °C. The pellet was resuspended with a buffer containing 50 mM MES-NaOH (pH

6.0), 150 mM NaCl, and 5 mM MgCl<sub>2</sub>, and resuspension was centrifuged at 4,000 × g for 10 min at 4 °C. The pellet was then resuspended with a buffer containing 50 mM MES-NaOH (pH 6.0), 15 mM NaCl, and 5 mM MgCl<sub>2</sub>, and resuspension was centrifuged at 6,000 × g for 10 min at 4 °C. The pelleted thylakoid membranes were resuspended with the same buffer, and the concentration of chlorophylls was quantified by using 80% (v/v) acetone as described previously.<sup>6</sup> The thylakoid membranes (2.1 mg Chl/mL) were solubilized with 3.75% (w/v) Triton X-100 for 20 min on ice. The solution was centrifuged at 3,500 × g for 5 min at 4 °C. The supernatant was collected and further centrifuged at 40,000 × g for 30 min at 4 °C. The pelleted PSII-enriched membranes were washed with the same buffer and centrifuged again at 40,000 × g for 30 min at 4 °C. The PSII-enriched membranes were resuspended with a buffer containing 50 mM MES-NaOH (pH 6.0), 15 mM NaCl, 5 mM MgCl<sub>2</sub>, and 400 mM sucrose, flash-frozen in liquid nitrogen, and stored at -80 °C until the following isolation procedures.

We isolated PSII-RC according to the previous literature with some modifications as follows.<sup>7-9</sup> The PSII-enriched membranes (1 mg Chl/mL) were solubilized with 4% (w/v) Triton X-100 in a buffer containing 50 mM Tris-HCl (pH 7.2) for 1 h on ice with gentle stirring. The solution was centrifuged at 33,000 × g for 1 h at 4 °C. The supernatant was collected and loaded onto an anion exchange column (Toyopearl DEAE-650S resin) which was equilibrated

with a buffer containing 50 mM Tris-HCl (pH 7.2), 30 mM NaCl, and 0.05% (w/v) Triton X-100 at 4 °C. The column was washed with the same buffer at a flow rate of 2.6 mL/min until the eluate showed the 417:435 nm ratio of about 1.16. Then, the column was subjected to a NaCl linear gradient from 30 to 200 mM at a flow rate of 1 mL/min. The green fraction eluted at 90-120 mM NaCl was collected. Then, polyethylene glycol 3350 was slowly added to the collected fraction at the final concentration of 0.325 g/mL, and the mixture was incubated for 30 min on ice with gentle stirring. The solution was centrifuged at  $31,300 \times g$  for 15 min at 4 °C. The pelleted PSII RC was resuspended with the buffer containing 50 mM Tris-HCl (pH 7.2), 0.4 M sucrose, 0.1% (w/v) n-dodecyl- $\beta$ -D-maltoside (Anatrace) prepared with D<sub>2</sub>O. The PSII-RC was flash-frozen and stored at -80 °C until 2DEV measurements.

For the spectroscopic experiments, the PSII-RC sample was mixed with glycerol-*d*<sub>8</sub> in a 80:20 (v/v) glycerol:PSII-RC ratio. The sample cell was constructed from two CaF<sub>2</sub> plates with a kapton spacer. The maximum optical density of the PSII-RC sample in the investigated visible range was set at ~1.0 with a path length of 200  $\mu$ m. The sample was placed in an optical cryostat (OptistatDN2, Oxford Instruments) at 77 K.

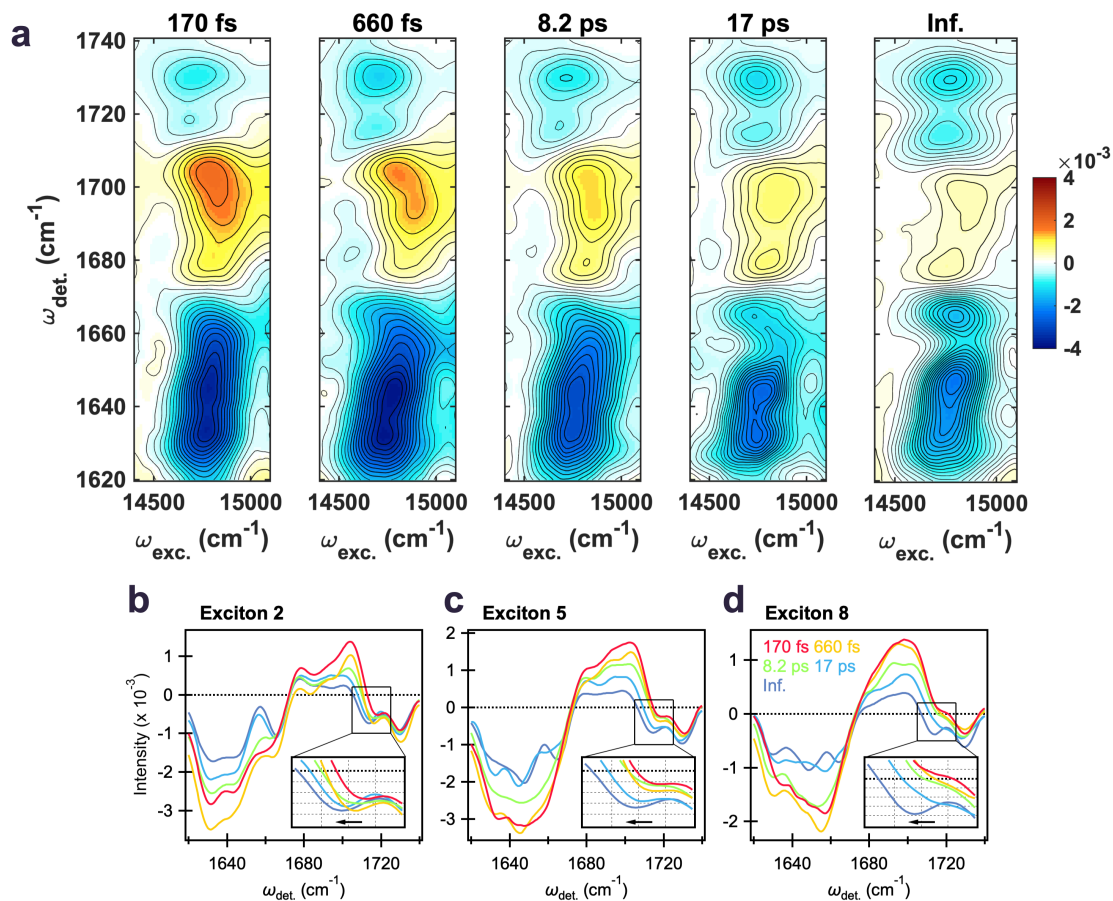


**Figure S1.** Two dimensional-evolution associated difference spectra (2D-EADS) of PSII-RC

(a). Five components were required for a reasonable fit with time constants of 170 fs, 660 fs, 8.2 ps, 17 ps and a non-decaying offset component (longer than current detection time range of 100 ps). Each 2D-EADS evolves into the next one with the time constants listed above. Contour levels are drawn in 5% intervals. The time-dependent evolution of excitons 2, 5, and 8 are shown in (b)-(d), respectively.



## References

1. Oliver, T. A. A., Lewis, N. H. C. & Fleming, G. R. Correlating the motion of electrons and nuclei with two-dimensional electronic-vibrational spectroscopy. *Proc. Natl. Acad. Sci.* **111**, 10061–10066 (2014).
2. Zhang, Z., Wells, K. L., Hyland, E. W. J. & Tan, H. S. Phase-cycling schemes for pump-probe beam geometry two-dimensional electronic spectroscopy. *Chem. Phys. Lett.* **550**, 156–161 (2012).
3. Fleming, G. R., Lewis, N. H. C., Arsenault, E. A., Wu, E. C. & Oldemeyer, S. Two-Dimensional Electronic Vibrational Spectroscopy. in *Coherent Multidimensional Spectroscopy* (ed. Cho, M.) 35–49 (Springer Singapore, 2019). doi:10.1007/978-981-13-9753-0\_2.
4. Berthold, D. A., Babcock, G. T. & Yocum, C. F. A highly resolved, oxygen-evolving photosystem II preparation from spinach thylakoid membranes. EPR and electron-transport properties. *FEBS Lett.* **134**, 231–234 (1981).
5. Caffarri, S., Kouřil, R., Kereïche, S., Boekema, E. J. & Croce, R. Functional architecture of higher plant photosystem II supercomplexes. *EMBO J.* **28**, 3052–3063 (2009).

6. Porra, R. J., Thompson, W. A. & Kriedemann, P. E. Determination of accurate extinction coefficients and simultaneous equations for assaying chlorophylls a and b extracted with four different solvents: verification of the concentration of chlorophyll standards by atomic absorption spectroscopy. *Biochim. Biophys. Acta - Bioenerg.* **975**, 384–394 (1989).
7. Nanba, O. & Satoh, K. Isolation of a photosystem II reaction center consisting of D-1 and D-2 polypeptides and cytochrome b-559. *Proc. Natl. Acad. Sci.* **84**, 109–112 (1987).
8. McTavish, H., Picorel, R. & Seibert, M. Stabilization of Isolated Photosystem II Reaction Center Complex in the Dark and in the Light Using Polyethylene Glycol and an Oxygen-Scrubbing System. *Plant Physiol.* **89**, 452–456 (1989).
9. Seibert, M. & Picorel, R. Isolation of Photosystem II Reaction Center Complexes from Plants. in *Photosynthesis Research Protocols* (ed. Carpentier, R.) 17–27 (Humana Press, 2011). doi:10.1007/978-1-60761-925-3\_3.